Granular transport in a horizontally vibrated sawtooth channel

Shahin Mobarakabadi,[1] Ehsan Nedaaee Oskoee,[1,*] Matthias Schröter,[2] and Mehdi Habibi[1,3,†]
[1]*Institute for Advanced Studies in Basic Sciences, Gava Zang, Zanjan 45195-159, Iran*
[2]*Max Planck Institute for Dynamics and Self-Organization (MPIDS), 37077 Göttingen, Germany*
[3]*Institute of Physics, University of Amsterdam, Science Park 904, Amsterdam, the Netherlands*
(Received 22 February 2013; revised manuscript received 26 June 2013; published 9 October 2013)

We present a new mode of transport of spherical particles in a horizontally vibrated channel with sawtooth-shaped side walls. The underlying driving mechanism is based on an interplay of directional energy injection transformed by the sidewall collisions and density-dependent interparticle collisions. Experiments and matching numerics show that the average particle velocity reaches a maximum at 60% of the maximal filling density. Introducing a spatial phase shift between the channel boundaries increases the transport velocity by an order of magnitude.

DOI: 10.1103/PhysRevE.88.042201 PACS number(s): 45.70.−n, 87.15.hj

I. INTRODUCTION

Brownian motors extract useful work from a noisy environment by means of a broken spatial symmetry [1,2]. The concept of Brownian motors is of great importance in cell biology and nanotechnology; however, their underlying principle is not limited to thermal noise and can therefore be also implemented in macroscopic setups. One example for such an athermal, macroscopic, and noisy environment are granular gases [3].

Due to the dissipative collisions between particles, granular gases require constant external driving, which is in most cases provided by shaking the container. Work can then, e.g., be extracted by means of a rotational ratchet, where the symmetry is broken by different coatings on the two sides of each vane [4]. Or probe particles with an asymmetric shape can be set into translational [5,6] or rotational [7] motion.

Another class of granular Brownian motors converts the random motion of the particles into a directed flow. This can either be implemented by breaking the symmetry of the driving [8–10] or by breaking the spatial symmetry of the container boundaries [11–18]. All setups in the latter group include a sawtooth-shaped base plate which is shaken vertically to drive the granular gas. Their phenomenology includes height-dependent flow directions [11–13,16], segregation of binary mixtures [14,15], and rotational motion of the circular base [17].

In this paper we decouple the direction of driving from gravity: our system is a horizontally vibrated channel where sawtooth-shaped side walls break the symmetry. This geometry allows us to control the average particle density, a feature which can not be realized with vertically shaken cells with a sawtooth floor. We observe unidirectional transport with a nonmonotone density dependence. In Sec. II we discuss the experimental setup and results. In Sec. III we introduce and validate our numerical simulations, which are then used in Sec. IV to gain insight into the transport mechanisms.

*nedaaee@iasbs.ac.ir
†habibi@iasbs.ac.ir

II. EXPERIMENTAL RESULTS

The experimental setup consists of two sawtooth corridors which are connected by two small pentagonal cells at each end of the corridors, as shown in Fig. 1(a). Each corridor consists of five triangular cells; both floor and walls are made from plexiglass. The channels are mounted horizontally and shaken in the x direction [cf. Fig. 1(b)] using an of-center pulley which is driven by an AC motor. The oscillations amplitude is 7.5 ± 0.5 mm, the driving frequency 5 Hz.

The channel is filled with steel spheres of radius 6 mm. The maximum number of spheres per triangular cell is 21; this value defines the maximal area fraction ϕ_c. Ten percent of the beads have been colored in order to use them as tracers; this has been achieved by oxidizing them in a fire for 1 min. We checked with a simple bouncing experiment that their restitution coefficient was within the error bar of untreated steel spheres. The average speed of the beads is then determined by measuring the rate at which tracers enter a given cell; the sample time is chosen so that the average tracer has completed at least two full cycles.

Figure 2 shows the average drift speed as a function of the renormalized area fraction (ϕ/ϕ_c) where ϕ is the number of spheres per cell. Three different regimes can be distinguished. For low area fractions ($0.005 \leqslant \phi/\phi_c < 0.08$) the particles move in a negative y direction [i.e., downward in Fig. 1(b)] with a velocity that is independent of ϕ. As here there are on average fewer than two beads in a cell, particle-particle collisions are rare. We refer to this range as the *dilute regime*.

For intermediate area fractions ($0.08 \leqslant \phi/\phi_c < 0.6$) the average speed increases monotonously. Fitting a line to the experimental data in Fig. 2 shows that $\langle V_y \rangle \sim (\phi/\phi_c)^{0.6(\pm 0.05)}$ in the intermediate regime. This effect delineates the *cooperative regime*.

For even higher densities ($\phi/\phi_c \geqslant 0.6$) the drift speed decreases sharply. As the system approaches the fluid-solid transition density, we refer to this as the *jamming regime*.

III. SIMULATION METHOD

To elucidate the transport mechanism we have performed molecular dynamics simulations. The normal force between

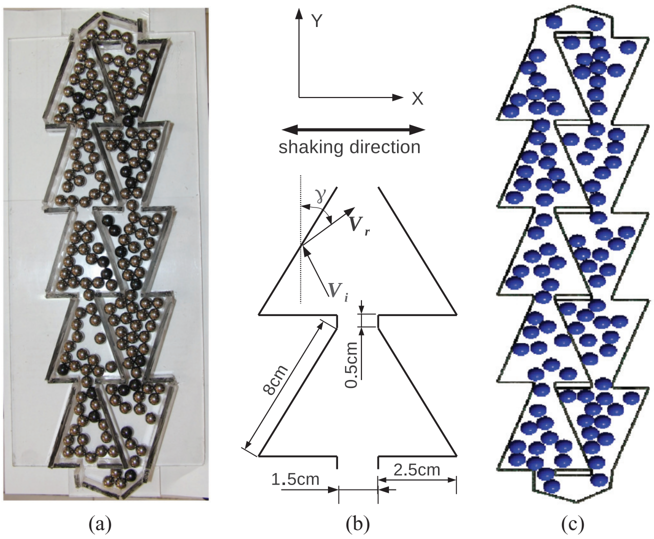

FIG. 1. (Color online) Sawtooth channel. Top view (a) and dimensions (b) of the experimental setup and visualization of the setup used in the simulations (c). Particles are transported in the negative y direction in panel (b).

two grains i and j, $\mathbf{F}_{n_{i,j}}$, is given by

$$\mathbf{F}_{n_{i,j}} = f\left(\frac{\delta_{i,j}}{d}\right)\left(k_n \delta_{i,j} \mathbf{n}_{i,j} - \gamma_n m_{\text{eff}} \mathbf{v}_{n_{i,j}}\right). \quad (1)$$

Here $\mathbf{v}_{n_{i,j}}$ is the normal component of the relative velocity between the grains (evaluated at the contact point). $\mathbf{n}_{i,j}$ is the unit vector corresponding to the distance $r_{i,j}$ between the two grain centers. d is the particle diameter, m_{eff} the effective mass $m_i m_j/(m_i + m_j)$, and $\delta_{i,j} = d - r_{i,j}$ is the normal compression at the contact. $f(x)$ equals $\sqrt{x}$, which models Hertzian contacts. The density of the grains is set to $7.87\ \text{g/cm}^3$. The numerical values of the elastic constant k_n and the viscoelastic constant γ_n are listed in Table I; they have been determined by numerically matching the experimental

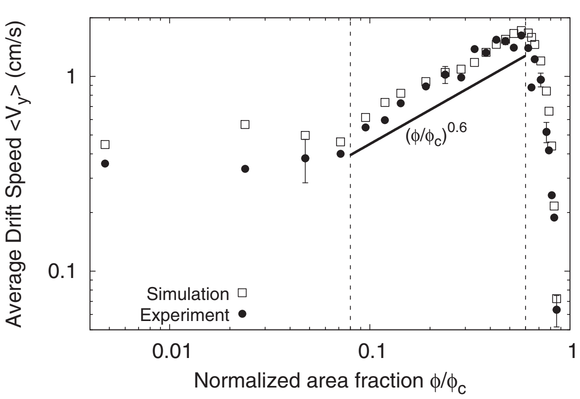

FIG. 2. Average drift speed as a function of the rescaled area fraction, measured in both experiment and simulation. Vertical dashed lines indicate the transition between the dilute (left), cooperative (middle), and jamming regime (right). The three example error bars are standard deviations over 10 cycles. The simulation time corresponds to the average particle performing four cycles. In both cases the oscillations amplitude is 7.5 mm and the driving frequency 5 Hz.

TABLE I. The numerical values of the contact model coefficients.

Coefficient	Numeric value	Coefficient	Numeric value
k_n	10^7 g/s^2	k_{nw}	10^7 g/s^2
γ_n	5×10^3 1/s	γ_{nw}	1.3×10^4 1/s
μ_s	0.5	μ_d	0.4

results of a steel sphere bouncing of a steel plate (respectively a plexiglass plate for the particle wall collisions described below).

We do neglect the the viscoelastic tangential interaction between grains; this ensures that particles do not experience any vertical forces and remain therefore in contact with the bottom surface of the channel. The agreement shown below between our simulations and experiments justifies this decision by hindsight.

The same equations are used to model the interaction between grains and the channel walls; the coefficients have an added subscript w. Viscoelastic tangential forces between the grains and side walls are neglected too. The mass of the container is set to be infinity; consequentially $m_{\text{eff}} = m$.

For the evaluation of the tangential force $\mathbf{f}$ exerted by the channel bottom on a particle we follow a method proposed by Kondic [19], which distinguishes between sliding and rolling contacts. In a first step the contact is assumed to be rolling with $\mathbf{f} = m\mathbf{a}$. Taking the rotation into account, the acceleration $\mathbf{a}$ of the sphere is taken in the frame of the laboratory and can be computed as $\mathbf{a} = 2/7\mathbf{a}_s$ with $\mathbf{a}_s$ being the acceleration of the surface. If the no-sliding condition $|\mathbf{f}| \leqslant f_{\max} = \mu_s mg$ (μ_s is the static coefficient of friction) is satisfied, this is the final result.

Otherwise, the sliding contact has to be evaluated using the dynamic friction coefficient μ_d:

$$\mathbf{f} = -\mu_d mg \frac{\mathbf{v}_w}{|\mathbf{v}_w|}, \quad (2)$$

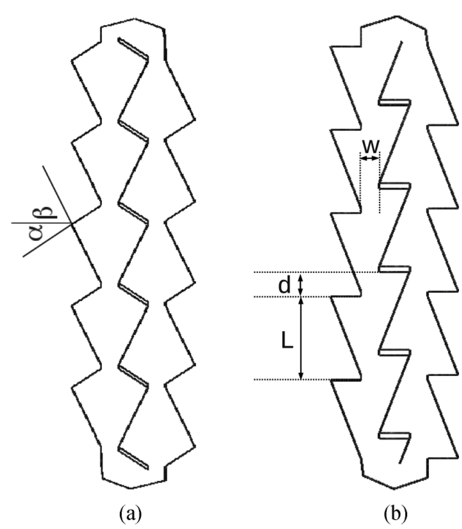

FIG. 3. Modified boundary geometries. Channel (a) interpolates between a sawtooth and a triangular shape by increasing the angle α. β is kept constant at 72° as in Fig. 1. Channel (b) introduces a relative displacement d of the two sidewalls.

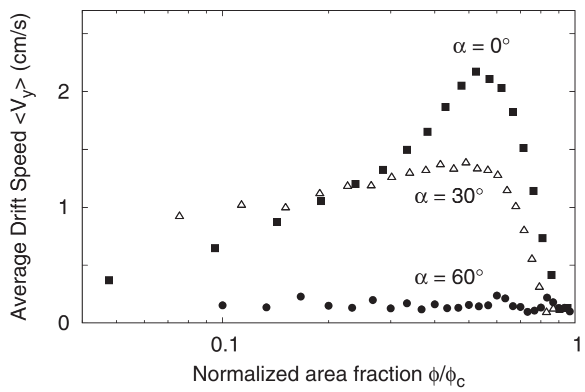

FIG. 4. The average drift speed depends on the asymmetry of the channel. These numerical data are measured in the setup shown in Fig. 3(a) at a shaking frequency of 6.4 Hz and an oscillation amplitude of 7.5 mm.

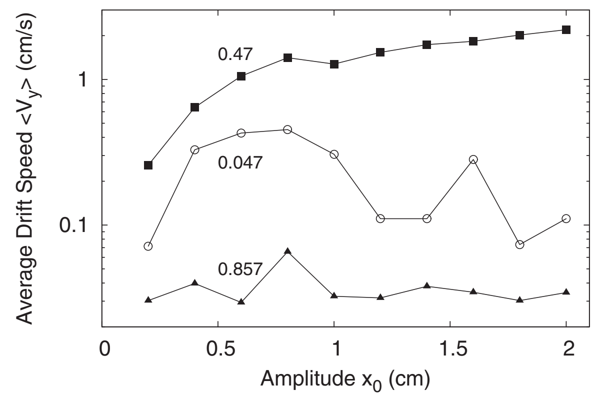

FIG. 6. Average drift speed versus shaking amplitude for three different values of ϕ/ϕ_c. The drift amplitude increases only in the cooperative regime with the driving strength. These numerical results are measured in the standard setup displayed in Fig. 1(c) with a driving frequency of 5 Hz.

where $\mathbf{v}_w$ is the velocity of the contact point relative to the substrate. The values of μ used are listed in Table I; they are justified only by their ability to reproduce the experimental results.

The shaking of the container is modeled by a sinusoidal excitation with an oscillation frequency ω and an amplitude x_0. As the simulations are performed in the referential frame of the container, a force $-\omega^2 x_0 \cos(\omega t)$ is added to each particle's center of mass. The code is written in C + + using a fifth-order predictor-corrector algorithm for numerical integration of the equations of motion. The time step increment (Δt) is set to 10^{-5} s in all simulations; the simulation time is chosen so that the average particle has performed four full cycles, which requires at maximum 3.6×10^7 time steps.

Figure 2 shows that the results of the simulation are in good agreement with the experiment. Therefore we will use our simulations to gain insight into the driving mechanism in the three regimes.

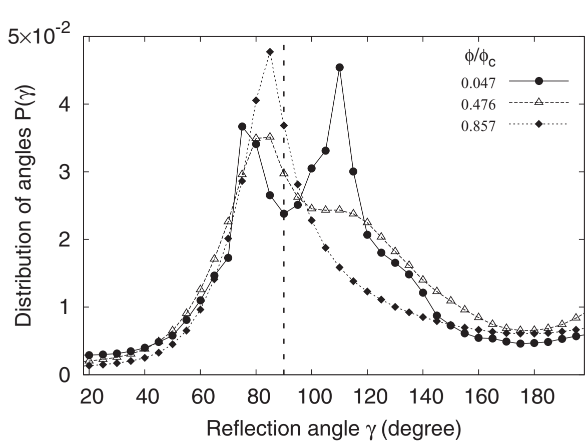

FIG. 5. Angular distribution of particle velocities after collisions with the sawtooth side walls. The angle γ is defined in Fig. 1(b). Values of γ between 90° and 198° make the particles go in the direction of the average drift. Numerical data measured with an oscillations amplitude of 7.5 mm and a driving frequency of 6.4 Hz.

IV. TRANSPORT MECHANISM

Understanding the transport mechanism depicted in Fig. 2 requires answers to the following three questions:

(A) Why are the particles moving unidirectionally at all? This is best discussed in the dilute regime.

(B) Why does the drift velocity increase in the cooperative regime?

(C) Why does the drift velocity go down at even higher densities?

A. Particles moving in the dilute regime

The dilute regime is specifically apt to study the underlying transport mechanism as it allows us to ignore interparticle collisions. First, it should be pointed out that dissipative collisions are not a necessary condition to have a finite drift velocity; the mechanism is therefore different from fluxes seen in granular gases going through beveled pores [20]. This has been tested by short simulations where γ_n and γ_{nw} have been set to zero.

Second, like in other ratchet systems the symmetry breaking of the boundary is a necessary condition to obtain a finite $\langle v_y \rangle$. If we increase in our simulations the angle α shown in Fig. 3(a), we change the channel profile from a sawtooth shape to a triangular one. This goes together with a reduction of the average drift velocity towards zero as shown in Fig. 4.

We therefore conjecture the following driving mechanism: spheres gain kinetic energy in the x direction due to the frictional contacts with the horizontally vibrating base. This kinetic energy is then converted by the sidewall collisions into a directed motion in the negative y direction. To substantiate this conjecture, we have computed the distribution P of the particle direction with respect to the y axis γ, measured after the particles collided with the sidewall [cf. Fig. 1(b)]. As can be seen in Fig. 5, the majority of postcollisional velocities point in a negative y direction, which corresponds to γ values larger than 90°. For $\phi/\phi_c = 0.047$ more than 60% of postcollision vectors fall into this range. Our system seems therefore in the dilute limit amenable for the analysis presented in Ref. [16], which would explain why for our comparatively elastic steel

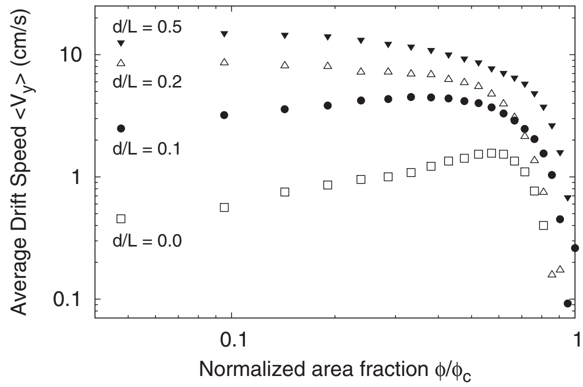

FIG. 7. Shifting the two sidewall by a distance d/L as displayed in Fig. 3(b) increases the average drift velocity by an order of magnitude and removes the transition between the dilute and the cooperative regime. Numerical data measured with an oscillations amplitude of 7.5 mm and a driving frequency of 5 Hz.

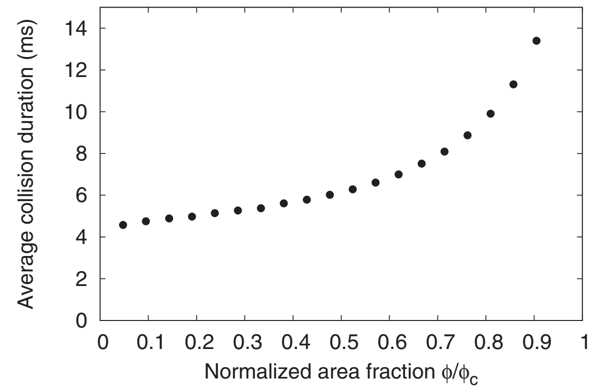

FIG. 8. The average collision duration doubles in the jamming regime, this hints towards the beginning formation of force chains. These numerical data are measured in the standard setup [Fig. 1(c)] with an oscillation amplitude of 7.5 mm and a driving frequency of 5 Hz.

particles and large ratchet angles no reversal of the transport direction was observed.

B. Cooperative regime

For values of $\phi/\phi_c > 0.08$, the average drift velocity increases proportional to $(\phi/\phi_c)^{0.6}$ as shown in Fig. 2. However, the postsidewall collision angle distribution $P(\gamma)$ even becomes more balanced; at $\phi/\phi_c = 0.476$ only 58% of the vectors point in a negative y direction. Therefore the mechanism behind the increase of $\langle v_y \rangle$ has to be something different. We hypothesize that the increased density keeps the particles longer in close proximity to the narrow passage between cells.

There are two indications for the importance of the narrow passage area. The first one can be seen in Fig. 6, which shows that $\langle v_y \rangle$ has (at all densities) a local maximum when the shaking amplitude x_0 is approximately half of the width of the passage. It is also interesting to note that only in the cooperative regime the average drift speed increases systematically with the amplitude x_0.

The second sign that improved overcoming of the narrow passage is the mechanism behind the cooperative regime can be found when studying a channel where the two sidewalls are shifted by a length d against each other as in Fig. 3(b). Figure 7 clearly demonstrates that the distinction between dilute and cooperative regime vanishes when the ratio d/L goes to 0.5, i.e., the narrow passages are taken out of the system. The accompanying increase of the average drift speed by one order of magnitude is also significant from the perspective of potential applications.

C. Jamming regime

The strong decrease in drift velocity for $\phi/\phi_c > 0.6$ can be explained back to two mechanisms. First, the effective redirection of the kinetic energy at the sidewalls stops. As can be seen in Fig. 5 at $\phi/\phi_c = 0.857$ only 49% of the postcollisional velocities have γ values larger than 90°.

Second, Fig. 8 shows that the average collision duration doubles in the jamming regime. For Hertzian single particles the collision duration is proportional to $v_n^{-0.2}$ [21]. As the kinetic energy of the particles decreases only by about 25% in the jamming regime, this dependence cannot explain the observed increase in the average collision duration. We hypothesize therefore that the emergence of short-lived but system-spanning force chains is responsible for this increase.

V. CONCLUSIONS

We have demonstrated experimentally and numerically a new method of granular transport in a horizontally vibrated channel with sawtooth-shaped boundaries. The average drift speed depends on the filling fraction, increasing for intermediate densities and decreasing again when approaching jamming. The underlying driving mechanism was found to be the redirection of the injected kinetic energy in the particle sidewall collisions. The reason for the drift speed increase at intermediate densities seems to be the improved flux through the narrow passages between the tips of the sawteeth; removing them by introducing a phase shift between the two boundaries resulted in a more than tenfold increase in drift velocity. At high densities the average contact duration increases, which indicates that the energy injection through the shaking bottom plate becomes significantly less efficient. However, more work will be needed for establishing a microscopic theory of this transport mechanism.

ACKNOWLEDGMENTS

We thank Y. Rahmani for his help in preparing the experimental setup and H. Fazli for helpful discussions. Support from the IASBS Research Council (Grants No. G2012IASBS103 and No. G2012IASBS106) is acknowledged.

[1] P. Hänggi and F. Marchesoni, Rev. Modern Phys. **81**, 387 (2009).
[2] P. Reimann, Phys. Rep. **361**, 57 (2002).
[3] N. V. Brilliantov and T. Pöschel, *Kinetic Theory of Granular Gases* (Oxford University Press, Oxford, 2004).

[4] P. Eshuis, K. van der Weele, D. Lohse, and D. van der Meer, Phys. Rev. Lett. **104**, 248001 (2010).
[5] B. Cleuren and C. Van den Broeck, Europhys. Lett. **77**, 50003 (2007).
[6] G. Costantini, U. M. B. Marconi, and A. Puglisi, Phys. Rev. E **75**, 061124 (2007).
[7] R. Balzan, F. Dalton, V. Loreto, A. Petri, and G. Pontuale, Phys. Rev. E **83**, 031310 (2011).
[8] J. A. Gallas, H. J. Herrmann, and S. Sokolowski, J. Phys. II **2**, 1389 (1992).
[9] R. Grochowski, P. Walzel, M. Rouijaa, C. A. Kruelle, and I. Rehberg, Appl. Phys. Lett. **84**, 1019 (2004).
[10] J. Blaschke and J. Vollmer, Phys. Rev. E **87**, 040201 (2013).
[11] I. Derényi, P. Tegzes, and T. Vicsek, Chaos **8**, 657 (1998).
[12] Z. Farkas, P. Tegzes, A. Vukics, and T. Vicsek, Phys. Rev. E **60**, 7022 (1999).
[13] M. Levanon and D. C. Rapaport, Phys. Rev. E **64**, 011304 (2001).
[14] Z. Farkas, F. Szalai, D. E. Wolf, and T. Vicsek, Phys. Rev. E **65**, 022301 (2002).
[15] J. F. Wambaugh, C. Reichhardt, and C. J. Olson, Phys. Rev. E **65**, 031308 (2002).
[16] A. Bae, W. Morgado, J. Veerman, and G. Vasconcelos, Physica A **342**, 22 (2004).
[17] M. Heckel, P. Müller, T. Pöschel, and J. A. C. Gallas, Phys. Rev. E **86**, 061310 (2012).
[18] K. H. Chen, Y. C. Chou, and K. To, Phys. Rev. E **87**, 012711 (2013).
[19] L. Kondic, Phys. Rev. E **60**, 751 (1999).
[20] R. S. Shaw, N. Packard, M. Schröter, and H. L. Swinney, PNAS **104**, 9580 (2007).
[21] T. Schwager and T. Pöschel, Phys. Rev. E **57**, 650 (1998).